Macromolecular Research
https://doi.org/10.1007/s13233-024-00312-3

Online ISSN 2092-7673
Print ISSN 1598-5032

ARTICLE

Lanthanide-doped zinc gallium oxide ($ZnGa_2O_4$) nanocrystals and their engineered photoluminescence

Kihyo Kim[1] · Kicheol Kim[1] · Hyo-Geun Kwon[1] · Sunghoon Kim[2] · Sang-Wook Kim[1]

Received: 31 May 2024 / Revised: 5 July 2024 / Accepted: 21 July 2024

Abstract

Zinc gallate ($ZnGa_2O_4$) has been introduced in various studies as a good host phosphorescent material, and the change of its optical properties by ion doping has received much attention. However, $ZnGa_2O_4$ is mostly synthesized through solid-state reactions, the reaction conditions of high temperature and pressure were required, and its low dispersibility often limited its applications. In this study, we synthesized normal spinel structured $ZnGa_2O_4$ nanocrystals through a colloidal method. Lanthanide doping specifically with europium and terbium resulted in red (614 nm, photoluminescence quantum yield (PLQY): 2.2%) and green (545 nm, PLQY: 13.6%) emissions under 254 nm UV excitation. By applying the novel co-doping system of europium and terbium to the synthesis of colloidal $ZnGa_2O_4$ for the first time, we were able to achieve various color conversions including green, red, and white by adjusting amount and ratio of lanthanide ions.

Graphic Abstract

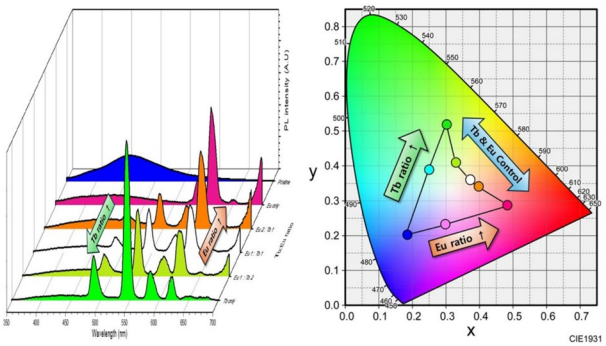

Keywords $ZnGa_2O_4$ · Colloidal synthesis · Lanthanide · Co-doping

1 Introduction

Zinc gallate ($ZnGa_2O_4$) is a phosphorescent material with a normal spinel (Fd3m space group, JCDPS: 38–1240) crystal structure [1]. In this spinel structure, zinc (Zn^{2+}) ions occupy the tetrahedral sites, while gallium (Ga^{3+}) ions occupy the octahedral sites. It is a well-known wide-bandgap material with a bandgap of approximately 4.4 eV, which allows it to emit light in the blue region when excited by UV light [2]. $ZnGa_2O_4$ has been reported in various studies as a good host material for phosphors. When blue emission from the host is transferred to transition metals or rare earth ions, such as lanthanides, it results in the emission of the characteristic colors of these elements [3]. This property has potential applications in fields, such as field emission displays (FED), LED encapsulant and bioimaging [4–8]. Several studies have reported dopant emission from $ZnGa_2O_4$. Transition metals, such as Mn^{2+} and Cr^{3+}, are used to achieve green and red emissions,

✉ Sang-Wook Kim
swkim@ajou.ac.kr

[1] Department of Molecular Science and Technology, Ajou University, Suwon 16499, Korea

[2] Department of Applied Chemistry Food Science and Technology, Dong-Eui University, Busan 47340, Korea

Published online: 13 August 2024

[9–11] respectively. Lanthanide ions, such as Eu^{3+} and Tb^{3+}, can be utilized as phosphorescent materials, emitting red and green light, respectively [12]. These materials exhibit a characteristic narrow emission spectrum through the 4f–4f or 4f–5d transitions [3]. Furthermore, the state of charge transfer corresponding to each photoluminescence (PL) peak has been precisely identified [11]. Color-tunable PL can be achieved by combining two or more elements. Combinations of Dy^{3+}, $Tb^{3+}$and Mn^{3+}/ Ho^{3+}, Bi^{3+} and Yb^{3+}/ Er^{3+}, Tb^{3+} and Yb^{3+} allow tuning of the emission color by varying the dopant composition [13–15]. In addition, a previous study reported that the co-doping of $ZnGa_2O_4$ with Eu^{3+} and Tb^{3+} achieved red, green, and white emissions [16] .

There are several methods for the synthesis of $ZnGa_2O_4$, including solid-state reactions, [8] sol–gel methods [10], polyol methods [12], hydrothermal methods [17], and co-precipitation and annealing [18]. Among these methods, the solid-state reaction is the most commonly used for synthesizing $ZnGa_2O_4$, which typically results in microsized particles with low dispersibility [19]. Other synthesis methods also lead to crystal aggregation and poor dispersibility in organic solvents. Colloidal $ZnGa_2O_4$ nanocrystals, which exhibit good dispersity in solvents, [3] have been reported as an improved method. Generally, colloidal method can provide dispersibility in organic solvent to the synthesized nanocrystals due to hydrophobic interaction between organic solvents and long alkyl chain of a surfactant attached to the surface of a nanoparticle. Enhancing dispersibility offers processability for display device fabrication and the possibility of a biomarker. However, the previous study focused on the single doping of europium and terbium, it was not possible to achieve color tunability by adjusting the lanthanide doping ratios. Therefore, we suggested the idea of double-doped $ZnGa_2O_4$, which can be dispersed in organic solvents and exhibits color tunability by adjusting the doping ratios of lanthanides.

In this study, $ZnGa_2O_4$ nanocrystals were synthesized using a previously reported colloidal method in an organic solvent, [3] rather than a solid-state method. Organic ligands were used to achieve dispersibility in organic solvents. Eu $^{3+}$ and Tb^{3+} were added to the $ZnGa_2O_4$ during the colloidal synthesis process, and the PL changes were analyzed. Moreover, the co-doping of Eu^{3+} and Tb^{3+} to $ZnGa_2O_4$ during the colloidal synthesis process was performed for the first time, and changes in the photoluminescence quantum yield (PLQY) and color tunability based on the doping ratio were elucidated using CIE chromatography diagrams.

2 Experimental

2.1 Materials

All chemicals, Zn(II) acetylacetonate hydrate ($Zn(acac)_2$, Sigma-Aldrich), Ga(III) acetylacetonate ($Ga(acac)_3$, 99.99% trace metal basis, Sigma-Aldrich), Eu(III) acetate hydrate ($Eu(OAc)_3{\cdot}xH_2O$, REacton®, 99.9%, Alfa), Tb(III) acetate hydrate($Tb(OAc)_3{\cdot}xH_2O$, REacton®, 99.9%, Alfa) 1,2-hexadecanediol (HDD, 90%, Technical grade, Sigma-Aldrich), benzyl ether (98%, Sigma-Aldrich), oleic acid (OA, 90% technical grade, Sigma-Aldrich), and oleylamine (OLA, 70% technical grade, Sigma-Aldrich) were used without further purification.

2.2 Synthesis of zinc gallium oxide ($ZnGa_2O_4$)

For the synthesis of pristine and lanthanide-doped $ZnGa_2O_4$, a previously reported colloidal synthesis method was used [3]. 1 mmol of $Zn(acac)_2$, 2 mmol of $Ga(acac)_3$, 5 mmol of HDD, 6 mmol of OA, and 6 mmol of OLA were added to 10 mL of benzyl ether and degassed in a three-neck reaction flask. By substituting the appropriate amount (0 to 0.3 mmol) of $Eu(OAc)_3{\cdot}xH_2O$ and $Tb(OAc)_3{\cdot}xH_2O$ for $Ga(acac)_3$, lanthanide-doped $ZnGa_2O_4$ could be synthesized. After degassing, it was filled with N_2 gas and heated to 200 °C for 30 min. The solution was heated to 280 °C for 30 min at N_2 flow. After the completion of the reaction, the solution was cooled to RT and diluted with hexane. The successfully synthesized $ZnGa_2O_4$ nanocrystals were precipitated by adding ethanol and collected by centrifugation at 8000 rpm for 10 min. After purification, $ZnGa_2O_4$ nanocrystals were dispersed in hexane for optical characterization**.**

2.3 Material characterization

Absorption spectra were measured using a Scinco PDA S-3100 UV–vis spectrophotometer. XRD studies were performed using a Rigaku Ultima diffractometer equipped with a Cu Kα radiation source (λ = 0.15418 nm) at the Ajou University Computing Center. TEM images were obtained using a JEM-2100F (JEOL) system operated at 200 kV at the Korea Advanced NanoFab Center. The absolute PLQY and PL emission spectra were measured using an FP-8500 instrument (Jasco) and an FS5 Spectrofluorometer (Edinburgh Instruments).

3 Results and discussion

3.1 Synthesis of $ZnGa_2O_4$

The formation of $ZnGa_2O_4$ nanoparticles was confirmed using XRD analysis. Figure 1a shows the XRD patterns of

$ZnGa_2O_4$ nanocrystals obtained by the colloidal method using a benzyl ether solvent and the synthesized $ZnGa_2O_4$ in which Ga^{3+} ions were replaced with lanthanides (Eu^{3+}, Tb^{3+}). The X-ray diffraction results showed that the diffraction peaks of the synthesized colloidal $ZnGa_2O_4$ matched well with those of bulk $ZnGa_2O_4$ [3]. (JCPDS File number: 38–1240, Fd3m, Cubic) The normal cubic spinel structure of $ZnGa_2O_4$, representing the Fd3m space group, has been reported to have Zn^{2+} ions occupying the tetrahedral sites and Ga^{3+} ions occupying the octahedral sites [1]. Among the measured diffraction peaks, the main diffraction peaks from (311) to (511) and (400) at 34.12°, 58.66°, and 62.86°matched well regardless of whether the Eu^{3+} or Tb^{3+} ions were doped. Since the diffraction peaks of pristine and lanthanide-doped $ZnGa_2O_4$ very slightly shift even in the bulk size, [16] the positions of the diffraction peaks in the nanosized pristine and lanthanide-doped $ZnGa_2O_4$ nanocrystals appear almost identical. The broader diffraction peaks compared to those of bulk $ZnGa_2O_4$ were attributed to the lower crystallinity resulting from the synthesis of nanosized crystals, as shown in Fig. 1b. Figure 1b shows the TEM images of Tb^{3+}-doped $ZnGa_2O_4$. Figure 1c also shows that the synthesized $ZnGa_2O_4$ nanocrystals exhibited an approximate size of 2.69 nm.

The synthesized nanocrystals showed unique optical properties. Figure 1d and e show the PL excitation spectrum and the energy diagrams of the luminescence mechanisms of pristine and Tb^{3+}-doped $ZnGa_2O_4$. $ZnGa_2O_4$ is generally reported to be an ultrawide bandgap material (approximately 4.4 eV) [2]. The synthesized $ZnGa_2O_4$ nanocrystals emitted broad blue light at approximately 460 nm under 254 nm UV light [20]. The sharp peak observed at 254 nm in the PL excitation spectrum was identified as the charge–transfer band, where energy was transferred from O^{2-} to Ga^{3+} ions occupying octahedral sites [3]. As shown in the energy diagram on the right, the transferred energy leads to the emission of blue light between 412 and 467 nm through ^5D to ^7F transitions. In the case of terbium (lanthanide) doping, energy transfer from $^5D_3$ to $^5D_4$ occurs, leading to green emission through transitions to the 7F band [20]. In the case of europium doping, the energy diagram is illustrated in Figure S1 [21]. The emission bands for each charge–transfer band are shown in Figs. 2 and 3.

3.2 Optical properties after lanthanide doping

Figure 2 illustrates the changes in optical properties resulting from the doping of $ZnGa_2O_4$ with Tb^{3+}. The PL emission and PL absorption spectra of $ZnGa_2O_4$ doped with 0.3 mmol of Tb^{3+} are presented in Fig. 2a. In the PL emission spectrum, a broad host-emission PL of $ZnGa_2O_4$ at approximately 450 nm and four sharp PL emissions of Tb^{3+} charge transfer can be observed. The sharp PL emission due to Tb^{3+} doping resulted in changes in the CIE 1931 chromatography coordinates from (x: 0.1850, y: 0.2027) of pristine $ZnGa_2O_4$ to (x: 0.30234, y: 0.51861) in Fig. 2b. Figure 2c show the PL excitation spectrum of Tb^{3+}-doped $ZnGa_2O_4$. The energy transfer from $^5D_4$

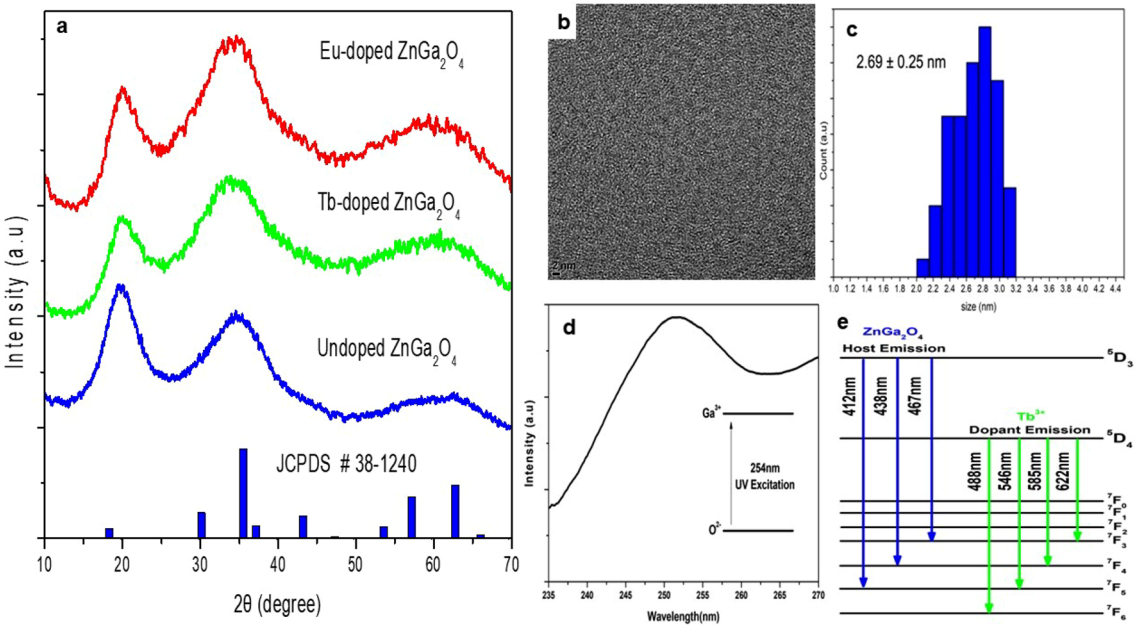

Fig. 1 (**a**) XRD pattern of pristine, Eu^{3+}-doped- and Tb^{3+}-doped $ZnGa_2O_4$ nanocrystals. (**b**) TEM images and (**c**) size distribution histogram of Tb^{3+}-doped $ZnGa_2O_4$ nanocrystals. (**d**) PL excitation spectra and (**e**) energy diagram for the luminescence mechanism of pristine and Tb^{3+}-doped $ZnGa_2O_4$ nanocrystals

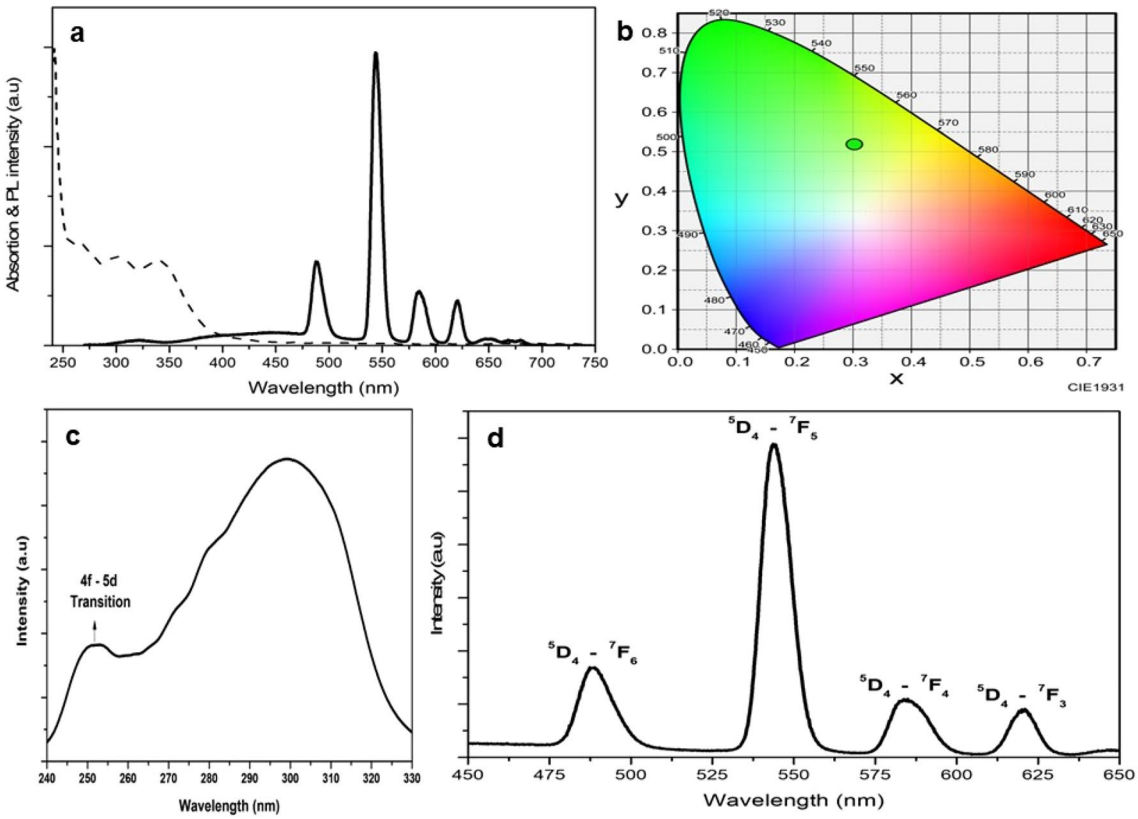

Fig. 2 (**a**) Absorption and PL emission spectra of Tb^{3+}-doped $ZnGa_2O_4$ nanocrystals. (**b**) The CIE 1931 chromatography diagram of Tb^{3+}-doped $ZnGa_2O_4$ nanocrystals. (**c**) PL excitation spectra and (**d**) PL emission spectra including charge transfer band of Tb^{3+} dopant emission

to ^7F_x, as indicated in the energy diagram of the emission mechanism in Fig. 1e, is reflected in the PL emission peaks shown in the emission spectrum in Fig. 2d [3, 21]. When Tb^{3+}-doped $ZnGa_2O_4$ exhibiting these optical properties was excited at 254 nm, a PLQY of 13.6% was measured.

Figure 3 illustrates the changes in optical properties resulting from doped $ZnGa_2O_4$ with Eu^{3+}, similar to the case with Tb^{3+}. The PL emission and PL absorption spectra of $ZnGa_2O_4$ doped with 0.3 mmol of Eu^{3+} are presented in Fig. 3a. The PL emission spectrum showed a broad host emission PL of $ZnGa_2O_4$ at approximately 450 nm and five sharp PL emissions of Eu^{3+} charge transfer. Figure 3c show the PL excitation spectrum of Eu^{3+}-doped $ZnGa_2O_4$. The charge–transfer bands from $^5D_0$ to ^7F_x are indicated for each PL emission peak in Fig. 3d [2, 3]. Doped $ZnGa_2O_4$ with Eu^{3+} also changed the CIE 1931 chromatography coordinates from zinc gallate to (x: 0.48311, y: 0.28751) in Fig. 3b. Comparing the charge transfer between Eu-doped- and Tb-doped zinc gallate with emission spectrum, Tb^{3+} zinc gallate demonstrate larger transfer property than Eu^{3+} zinc gallate. In addition, the PLQY of the Eu^{3+}-doped $ZnGa_2O_4$ was 2.2%, which was 10% lower than that of the Tb^{3+}-doped $ZnGa_2O_4$.

3.3 Color tunability after lanthanide doping

Through the luminescence mechanism described in Figs. 2 and 3, color tunability was achieved by adjusting the Eu^{3+} and Tb^{3+} doping ratios in $ZnGa_2O_4$. As the Tb^{3+} doping ratio increased, the intensities of the PL emission peaks at 488 and 545 nm, corresponding to the $^5D_4$ to $^7F_6$ and $^7F_5$ transitions, respectively, also increased. Conversely, as the Tb^{3+} doping ratio decreased and the Eu^{3+} doping ratio increased, the intensities of the PL emission peaks at 590 and 615 nm, corresponding to the $^5D_0$ to $^7F_1$ and $^7F_2$ transitions, gradually increased. Figure 4 illustrates the changes in the PL emission spectrum owing to variations in the doping ratios [16].

The broad host-emission of pristine $ZnGa_2O_4$ at approximately 450 nm was transferred to sharp emission bands when singly doped with lanthanide elements because of the specific energy transfer of each element, as shown in Figs. 2 and 3. By adjusting the Eu^{3+}:Tb^{3+} ratio to 1:2, 1:1, and 2:1, the intensities of the PL peaks emitted by each lanthanide element increased or decreased accordingly. While Eu^{3+} showed five sharp PL emission peaks and Tb^{3+} showed four emission peaks in the visible range, co-doped $ZnGa_2O_4$ did not exhibit a total of nine peaks in

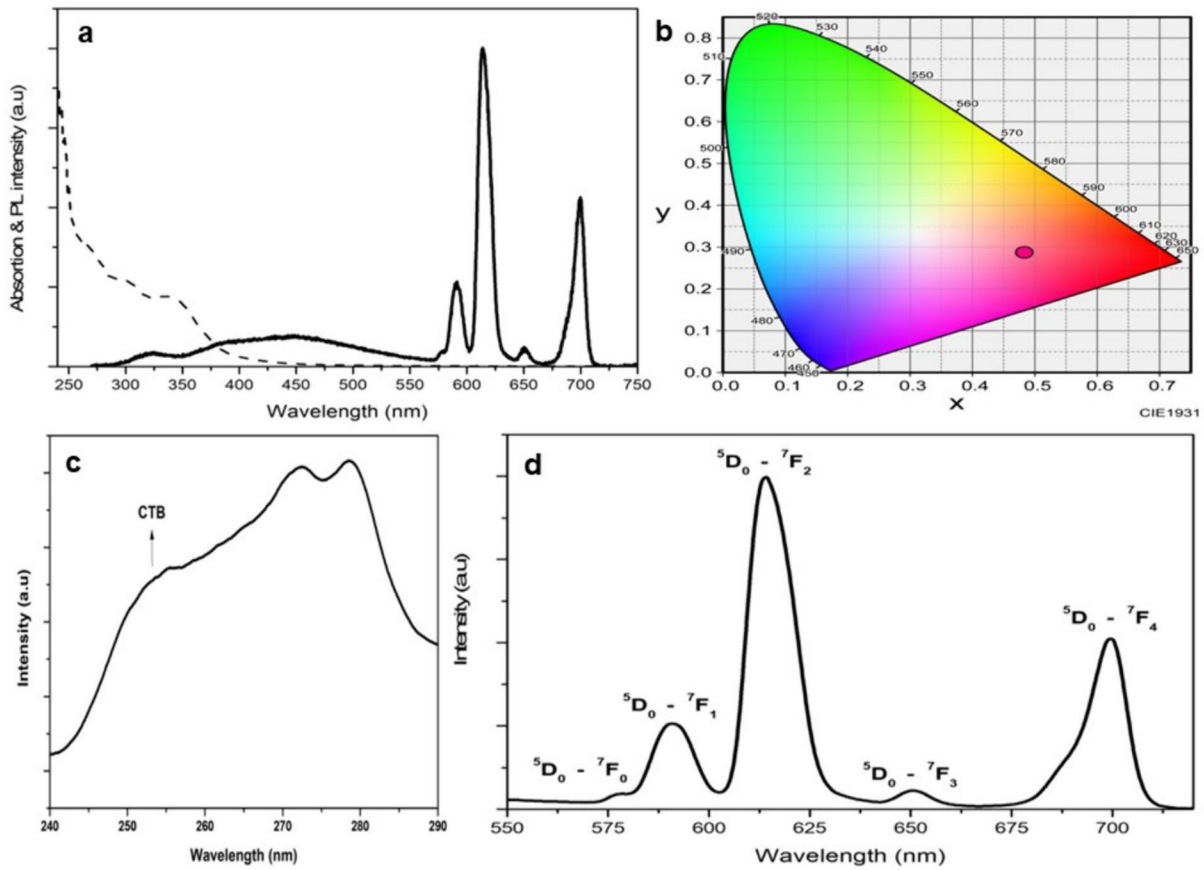

Fig. 3 (**a**) Absorption and PL emission spectra of Eu^{3+}-doped $ZnGa_2O_4$ nanocrystals. (**b**) The CIE 1931 chromatography diagram of Eu^{3+}-doped $ZnGa_2O_4$ nanocrystals. (**c**) PL excitation spectra and (**d**) PL emission spectra including charge transfer band of Eu^{3+} dopant emission

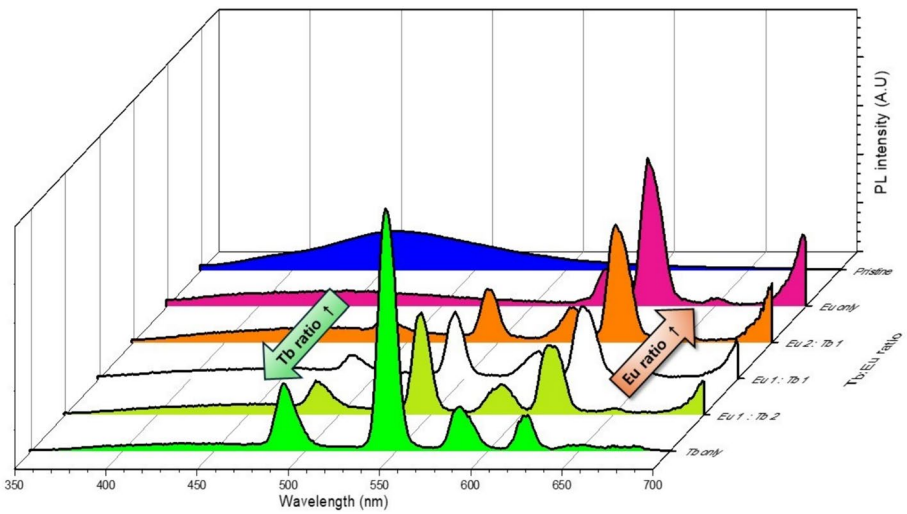

Fig. 4 PL emission spectra by adjusting the ratios of Eu^{3+} and Tb^{3+} doping

the spectrum. This is due to the spectral overlap caused by the energy transfer, resulting in the modulation of specific spectrum positions. This tendency is particularly evident in the emission peaks between 575 and 625 nm, as illustrated in Figure S2.

Figure 5 presents the photographs of the luminescence under a 254 nm UV lamp in a dark room, visually confirming the color tunability observed in the CIE 1931 chromatography diagram. Additionally, the PLQY values for $ZnGa_2O_4$ doped with Eu^{3+} and Tb^{3+} were 2.2% and 13.6%,

respectively, upon 254 nm UV excitation. For co-doped $ZnGa_2O_4$, the PLQY values exhibited a linear increase as the ratio of Eu^{3+} decreased and the ratio of Tb^{3+} increased.

The color tunability could linearly cover the CIE 1931 chromatography diagram when the lanthanide concentration was fixed at 0.3 mmol. Furthermore, by adjusting the doping amounts of Eu^{3+} and Tb^{3+} based on pristine $ZnGa_2O_4$ and lanthanide-doped $ZnGa_2O_4$, a broad area can be covered. Figure 6 shows the color coordinates from pristine $ZnGa_2O_4$ to $ZnGa_2O_4$ doped with 0.1 mmol and 0.3 mmol lanthanide. Both 0.1 mmol samples of Eu^{3+} and Tb^{3+} exhibit color coordinates between those of pristine $ZnGa_2O_4$ and 0.3 mmol samples. This demonstrates a system in which colors within the marked CIE chromatography area can be obtained by varying the amount and ratio of Eu^{3+} andTb^{3+} lanthanide dopant.

The main advantage of this study can be shown in the application of $ZnGa_2O_4$ as a display material. As shown in Fig. 6, the lanthanide doping of $ZnGa_2O_4$ resulted in significant coverage on the color coordinate diagram. For display materials, the ability of a single material to exhibit color tunability is crucial for uniformity and productivity. For example, CdSe quantum dots (QDs) have attracted significant interest owing to their high PLQY and color purity in the visible spectrum [22]. From this perspective, the color tunability of co-doped $ZnGa_2O_4$, which covers the RGB range as a single source, has great potential. Specifically, co-doped $ZnGa_2O_4$ offers significant advantages in display devices

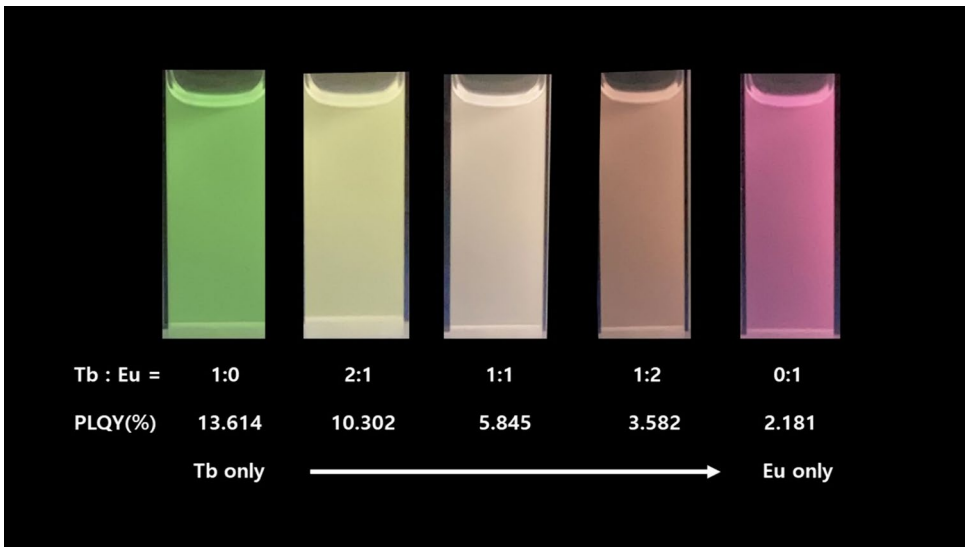

Fig. 5 Photographs of the luminescence under a 254 nm UV lamp in a dark room and changes of PLQY by adjusting the ratios of Eu^{3+} and Tb^{3+} doping

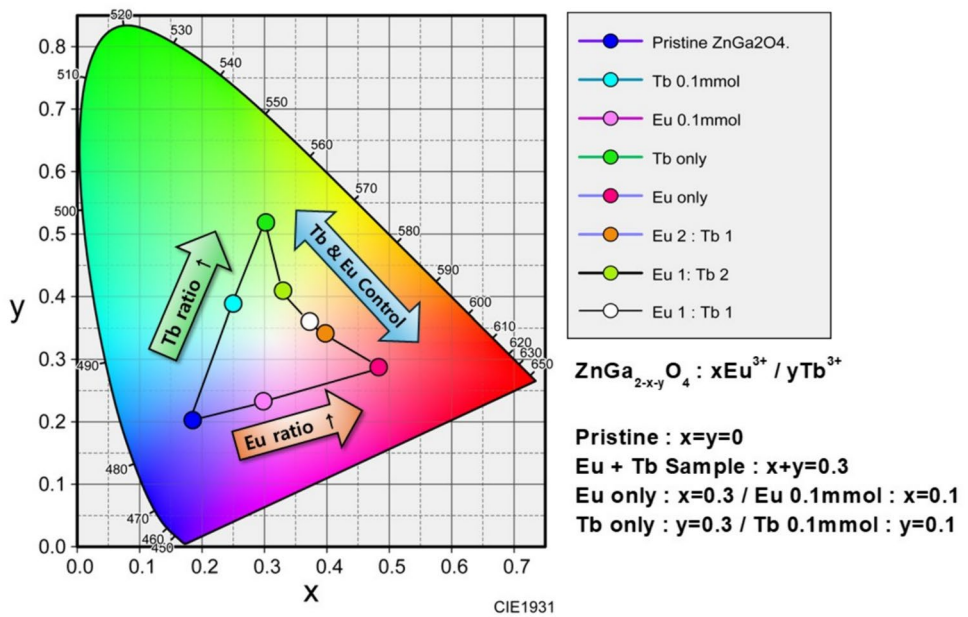

Fig. 6 The CIE 1931 chromatography diagram of Eu^{3+}, Tb^{3+} co-doping system of $ZnGa_2O_4$ nanocrystals

in terms of process uniformity compared to using different materials for RGB. Utilizing a single material provides significant benefits in terms of uniform lifetime, affinity for processing materials, and better control over surface conditions. Furthermore, through previously reported ligand engineering techniques, $ZnGa_2O_4$ could potentially be applied in fields such as display patterning and bioimaging [23, 24].

4 Conclusions

We successfully synthesized co-doped $ZnGa_2O_4$ nanocrystals with Tb^{3+} and Eu^{3+} ions for the first time using a colloidal synthesis method. The synthesized $ZnGa_2O_4$ material exhibited distinct luminescent properties corresponding to each lanthanide element when excited using 254 nm UV light. In addition, we demonstrated the ability to control optical properties by adjusting the ratio and amount of doped lanthanide ions. As the ratio of lanthanide ions changed, the intensity of the specific emission bands varied linearly, enabling the coverage of the area in the CIE 1931 chromatography diagram. The potential applications of this material in the display field are numerous, particularly as an LED encapsulation material. The ability of doped $ZnGa_2O_4$ to emit a wide range of colors as a single material offers substantial advantages in terms of process convenience and material uniformity for device fabrication. This study paves the way for the broader utilization of $ZnGa_2O_4$ in various display technologies owing to its unique optical properties.

Supplementary Information The online version contains supplementary material available at https://doi.org/10.1007/s13233-024-00312-3.

Acknowledgements This research was supported by a grant from the National Research Foundation of Korea (NRF) funded by the Korean government. (Ministry of Science and ICT) (2023R1A2C1003608)

References

1. R.S. Monika, A.B. Yadav, S.B. Rai, RSC Adv. **13**, 20164 (2023)
2. T.A. Safeera, E.I. Anila, Scripta Mater. **143**, 94 (2017)
3. H.-J. Byun, J.-U. Kim, H. Yang, Nanotechnology **20**, 495602 (2009)
4. M.-I. Chen, A.K. Singh, J.-L. Chiang, R. Horng, D. Wuu, Nanomaterials **10**, 2208 (2020)
5. Y. Liu, T. Zheng, X. Zhang, C. Chen, Sci. Rep. Rep. (2023). https://doi.org/10.1038/s41598-023-33498-0
6. T. Lecuyer, E. Teston, G. Ramirez-Garcia, T. Maldiney, B. Viana, J. Seguin, N. Mignet, D. Scherman, C. Richard, Theranostics. **6**, 2488 (2016)
7. T. Maldiney, B. Ballet, M. Bessodes, D. Scherman, C. Richard, Nanoscale **6**, 13970 (2014)
8. J.-H. Lee, H.-J. Park, Y. Kang, B.-W. Kim, J.C. Lee, S. Park, J. Eur. Ceram. Soc. **27**, 965 (2006)
9. T. Minami, T. Maeno, Y. Kuroi, S. Takata, Jpn. J. Appl. Phys. **34**, 684 (1995)
10 M.K. Hussen, F.B. Dejene, G.G. Gonfa, Appl. Phys. A (2018). https://doi.org/10.1007/s00339-018-1796-x
11. H. Liu, F. Ren, H. Zhang, Y. Han, H. Qin, J. Zeng, Y. Wang, Q. Sun, Z. Li, M. Gao, J. Mater. Chem. B. **6**, 1508 (2018)
12. C.M. Rao, V. Sudarsan, R.S. Ningthoujam, U.K. Gautam, R.K. Vatsa, A. Vinu, A.K. Tyagi, J. Nanosci. Nanotechnol.Nanosci. Nanotechnol. **8**, 5776 (2008)
13. D.P. Dutta, R. Ghildiyal, A.K. Tyagi, J. Phys. Chem. C **113**, 16954 (2009)
14 R.S. Monika, A.R. Yadav, S.B. Rai, Sci. Rep. Rep. (2021). https://doi.org/10.1038/s41598-020-80364-4
15 Y. Cheng, K. Sun, Opt. **59**, 756 (2020)
16 E. Monika, A.B. Rai, S.B. Rai, J. Solid State Chem. **325**, 124159 (2023)
17. L. Chen, Y. Liu, Z. Lu, K. Huang, Mater. Chem. Phys. **97**, 247 (2006)
18. G. Sridhar, D. Hebbar, S.G. Menon, P.M. Lewis, K.S. Choudhari, R.E. Kroon, H.C. Swart, S.D. Kulkarni, Opt. Mater. **123**, 111919 (2021)
19. Y. Cheng, K. Sun, P. Ge, Opt. Mater. **83**, 13 (2018)
20. T.A. Safeera, E.I. Anila, J. Alloy. Compd. **764**, 142 (2018)
21. G.B. Nair, S.J. Dhoble, J. Fluoresc. **26**, 1865–1873 (2016)
22. B.O. Dabbousi, J. Rodriguez-Viejo, F.V. Mikulec, J.R. Heine, H. Mattoussi, R. Ober, K.F. Jensen, M.G. Bawendi, J. Phys. Chem. B **101**, 9463 (1997)
23. J. Yang, J. Yoo, W.S. Yu, M.K. Choi, Macromol. Res. **29**, 391 (2021)
24. D.K. Lee, Y.-K. Lee, Macromol. Res. Res. **18**, 641 (2010)